Progress In Electromagnetics Research C, Vol. 154, 47–59, 2025

PIER C

(Received 25 January 2025, Accepted 12 March 2025, Scheduled 24 March 2025)

Biomedical Antenna Design Optimization Using Multi-Objective Inverse Neural Networks

Rania Ibtissam Ben Melouka[1,*], Yamina Tighilt[2], Chemseddine Zebiri[1], Kamil Karaçuha[3], Abdelhak Ferhat Hamida[2], Arwa Mashat[4], and Nail Alaoui[5]

[1]*Laboratoire d'Electronique de Puissance et Commande Industrielle (LEPCI), Department of Electronics University of Ferhat Abbas, Setif-1, Setif 19000, Algeria*
[2]*Laboratoire d'Instrumentation Scientifique (LIS), Department of Electronics, Faculty of Engineering, University of Ferhat Abbas Setif-1, Setif 19000, Algeria*
[3]*Electrical Engineering Department, Istanbul Technical University, Istanbul, Turkey*
[4]*Department of Information Systems, Faculty of Computing and Information Technology, King Abdulaziz University P. O. Box 344, Rabigh 21911, Saudi Arabia*
[5]*Laboratoire de Modélisation, Simulation et Optimisation des Systèmes Complexes Réels University of Djelfa, Djelfa 17000, Algeria*

ABSTRACT: A new approach based on an Inverse Artificial Neural Network (IANN) for Multi-Objective Antenna design is presented in this paper. The network sets geometrical variables as the output and uses three antenna performances as inputs. The proposed ANN model is structured into two distinct parts: In the first part, three autonomous branches establish the correlation among the S parameters, gain, specific absorption rate (SAR), and geometric variables of the antenna. The outputs of these branches are used as input in the second part to derive a distinctive solution for these geometric variables. The proposed antenna dimensions are $20 \times 24 \times 1.58\,\mathrm{mm}^3$, and an ultra-wideband of 4.1 GHz to 8.7 GHz is achieved in free space and on human tissue, which coincides with the 5.8 GHz ISM band. Body temperature and specific absorption rate are simulated using the suggested rectangular patch antenna. The resulting optimized antenna holds promising potential for biomedical applications.

1. INTRODUCTION

Wireless Communications have become a vital part of biomedical applications. These technologies facilitate remote patient monitoring, telemedicine consultations, and telehealth services [1]. The performance of a wireless communication system in biomedical applications is highly dependent on the performance of antennas. In fact, antenna is a fundamental component to enable reliable transmission and reception of data either inside the human body or between medical devices placed on the body and external systems. However, designing antennas for biomedical applications poses specific challenges, namely achieving the desired performance while ensuring compatibility with biological tissues and minimizing their power absorption [2–5]. Methods for antenna synthesis and analysis encompass a wide range of techniques used in the design, modeling, and evaluation of antenna systems performances. Initially, numerical techniques such as the method of moments (MoM) [6], Finite Element Method (FEM) [7], and Finite Difference Time Domain (FDTD) [8] are difficult to program for complex structures. For this, many software tools are used to solve the problem of numerical techniques, such as CST Microwave Studio, HFSS (High-Frequency Structure Simulator), and FEKO. However, when electromagnetic (EM) structure design and optimization are employed, it often takes a large amount of CPU time to find the optimal design space parameters [9–11]. To overcome these difficulties, researchers have increasingly turned to advanced and faster optimization techniques, including genetic algorithms (GA), particle swarm optimization (PSO) [12], and artificial neural networks (ANNs).

Over the last three decades, ANNs have emerged as a powerful tool, inspired by the complex interconnected structure of the human brain [13]. This technique excels at capturing intricate relationships within data and is well suited for optimization tasks in antenna design and EM modeling. Various artificial neural network models have been proposed for the analysis and/or synthesis of antenna design [14–20].

In tandem with ANNs, multi-objective optimization algorithms have become pivotal for achieving better performance in antenna design. Techniques such as the firefly algorithm (FFA) and particle swarm optimization (PSO) have been enhanced for multi-parameter optimization, leading to improved performance in antenna designs [21, 22]. Neural networks are also used to determine the geometric parameters of a device by imposing the desired performance as inputs, which is called ANN reverse modeling and is used in [23] to design a microwave filter and in [24] to design a Fabry-Perot resonator antenna using ANN multiparameter modeling in conjunction with the support machine vector (VSM) data-classification technique. An extreme learning machine (ELM) is used in [25] to achieve sat-

* Corresponding author: Rania Ibtissam Ben Melouka (raniaibtissam.benmelouka@univ-setif.dz).

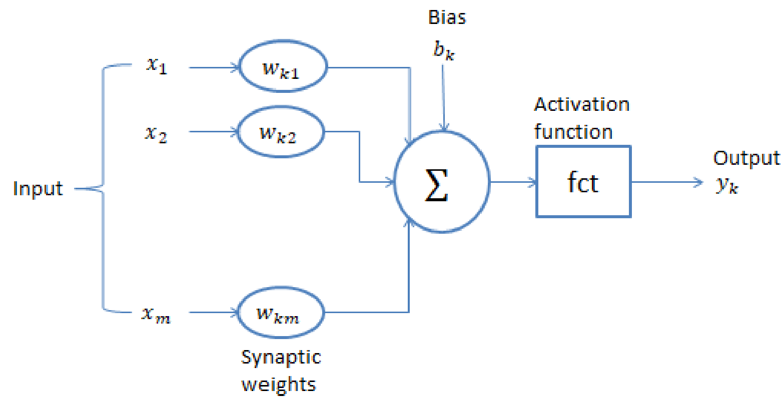

FIGURE 1. Artificial neural network [35].

isfactory geometry for parametric modeling of metasurfaces. In [26], a multi-objective problem of antenna design is solved using ANN reverse modeling where S-parameter, gain, and radiation pattern are set as inputs and the antenna geometric parameters as outputs. For reliable operation of a wireless communication system, the design of the antenna must meet multi-objectives simultaneously, namely: frequency band, gain, efficiency, radiation pattern, and for the particular case of biomedical applications, a Dielectric Assessment System (DAS) is added. However, the current literature lacks studies specifically focused on the Specific Absorption Rate (SAR) in biomedical antenna design using artificial intelligence [27–32]. In addition, the major problem that multiobjective modeling faces is the increase in learning cost with the increase of objectives [26]. Several techniques have been proposed to remedy this problem, as in [25], where the extreme learning machine (ELM) is used. In this paper, we propose a novel multi-objective inverse artificial neural network (MOIANN) approach to optimize antenna design parameters. Unlike conventional optimization methods, our approach directly predicts the geometric dimensions of the antenna based on specified performance criteria. This method significantly reduces calculation time by eliminating the need for iterative optimization processes. The other particularity of this paper is the introduction of SAR as a critical performance parameter for biomedical applications.

The paper is organized as follows. Section 2 provides a brief introduction to the ANN model. In Section 3, we explore various applications in antenna design, including free space, with tissue, and with tissue inverse, based on the appropriate antenna dimensions. Section 4 presents a comparison of results obtained using HFSS and the MATLAB-ANN toolbox across three different models. Finally, section 5 concludes the paper.

2. ANN MODEL

Artificial Neural Networks (ANNs) can be used as computational counterparts to the biological nervous system, drawing inspiration from its intricate architecture. These networks consist of interconnected units, working collectively to solve a wide array of problems. Within the realm of ANNs, several distinct types deserve consideration [32]. There are different types of feed-forward ANNs mentioned in [33]. The context of our approach is the use of a Multi-Layer Perceptron Neural Network (MLPNN). The choice of the learning algorithm holds utmost importance and warrants meticulous testing. Leveraging the versatile tools provided by MATLAB, which offers a diverse array of algorithms, we developed a MATLAB program. The Levenberg-Marquardt (LM) algorithm is used by this program to speed up the learning process. Several optimization algorithms were tested in [34] to train the artificial neural network (ANN), and the results showed that the LM algorithm was the most effective because it produced the most accurate results in the shortest time and fewest iterations.

Figure 1 presents the artificial neural network. The output y_k is determined by the weighted sum of the inputs x_m and bias b_k. The bias nodes are always set to one.

$$Y_k = \text{Fct}\left(\left(\sum_{j=1}^{m} w_{kj}x_j\right) + b_k\right) \tag{1}$$

Fct, the activation function, also known as the transfer function, is one of several activation functions that restrict the amplitude of the neuron's output, such as hyperbolic tangent, sigmoid, tanh, rectified linear unit (ReLU), leaky ReLU, and noisy ReLU [36].

2.1. The First Model

In this study, an artificial neural network model is developed to predict the geometrical parameters of a microstrip antenna based on simulation data. The ANN model consists of three independent neural networks, each designed to process different input features. As shown in Figure 2, the first ANN receives 101 values of S_{11}, simulating 101 frequency steps spreading from 0.6 GHz to 10.6 GHz with a step of 0.1 GHz as inputs and predicting six geometrical parameters as outputs. The second ANN is trained on gain-related parameters for the same number and nature of inputs and outputs, while the third ANN utilizes SAR values as input. Each ANN model consists of two hidden layers of five neurons in each one. A MATLAB program was developed to implement the model, integrating nine different optimization algorithms. Among them, the Levenberg-

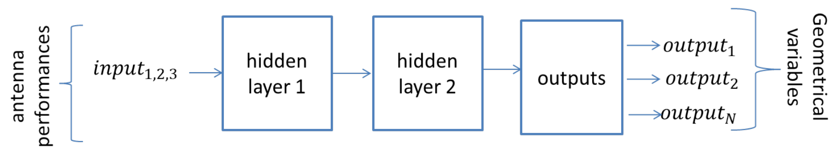

FIGURE 2. Inverse artificial neural network with separate inputs.

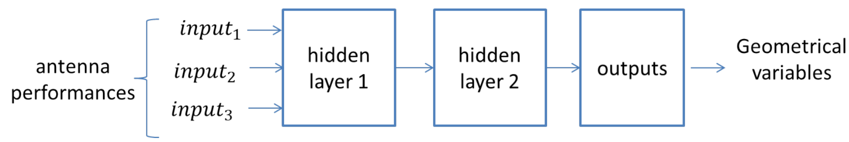

FIGURE 3. Inverse artificial neural network with non-separated inputs.

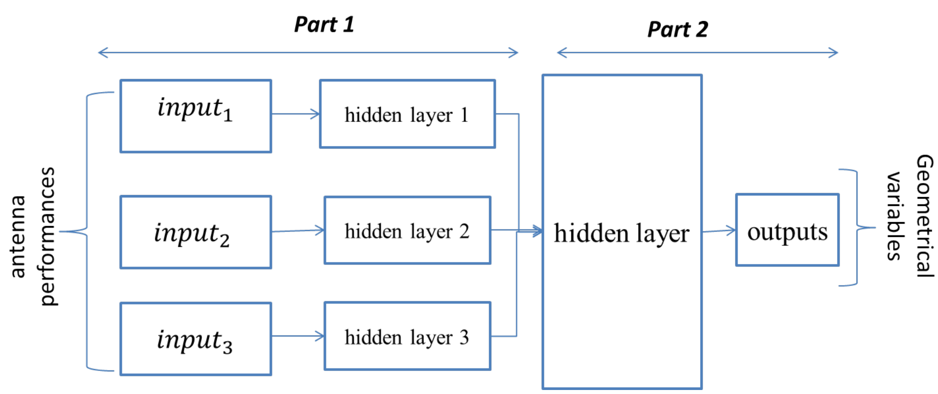

FIGURE 4. The proposed inverse neural networks.

Marquardt algorithm demonstrated the highest accuracy and efficiency [34]. The simulation-based generated data set is partitioned as follows: 70% for training, 15% for validation, and 15% for testing. Performance evaluation is conducted using mean squared error (MSE) metrics to assess prediction accuracy. After training, each ANN is tested on an independent data set, and here, new S_{11}, gain, and SAR values are fed into their respective networks to predict antenna geometrical parameters.

2.2. The Second Model

In the second model, the 101 values of the S_{11} parameter, gain, and SAR corresponding to each frequency step are used as inputs simultaneously for a single ANN model as shown in Figure 3. The ANN architecture includes (3×101) inputs, two hidden layers with five neurons in each layer to predict the six geometrical parameters or outputs of the considered design. The training process employs the Levenberg-Marquardt algorithm (trainlm). Model performance is assessed through statistical error metrics, particularly RMSE, ensuring high accuracy and reliability for antenna design optimization.

2.3. The Third Model (Proposed Model)

The proposed model is a partially connected neural network and consists of two parts. The first part consists of three branches. The second part consists of one fusion layer, as illustrated in Figure 4.

Part I: Three Parallel Branches

Branch 1 (S_{11} Features Processing): This branch establishes the local connection between the S_{11} parameters and geometrical parameters of the design.

- **Input Layer:** The inputs of this layer consist of the S_{11} parameters extracted from the dataset.
- **Locally Connected Layer 1:** Apply independent feature extraction operations on S_{11} values without shared weights. Five neurons are used in this layer.
- **Activation Layer 1:** Apply a nonlinear activation function, and in this case study, we used the sigmoid activation function.

Branch 2 (Gain Features Processing): This branch establishes the local connection between the antenna maximum gain and the geometrical parameters of the design.

- **Input Layer:** The inputs of this layer consist of the maximum gain extracted from the data set.
- **Locally Connected Layer 1:** Apply independent feature extraction operations on the gain values without shared weights. Five neurons are used in this layer.
- **Activation Layer 1:** Apply a nonlinear activation function, and in this case study, we used the sigmoid activation function.

Branch 3 (SAR Features Processing): This branch establishes the local connection between the SAR and geometrical parameters of the design.

- **Input Layer:** The inputs of this layer consist of the SAR extracted from the data set.
- **Locally Connected Layer 1:** Apply independent feature extraction operations on SAR values without shared weights. Five neurons are used in this layer.
- **Activation Layer 1:** Apply a nonlinear activation function, and in this case study, we used the sigmoid activation function.

Part II: Fusion Layer and Fully Connected Network

- **Fusion Layer:** Combine outputs from all three branches, aggregating information from S_{11}, gain, and SAR data.
- **Fully Connected Layers:** A sequence of dense layers with a hidden structure of [5, 5, 5, 5], optimizing the extracted features.
- **Output Layer:** Predict the desired parameters that correspond to the optimized antenna geometrical parameters.

The proposed inverse model comprises five distinct layers. The initial segment encompasses an input layer containing three independent blocks corresponding to S-parameters, independent gain values, and SAR. Following this, the first hidden layer and the first output layer are strategically employed to establish a mapping between the three performance indices and the associated geometrical variables. The subsequent segment of the model encompasses the Fourth and Fifth layers: a Second Hidden layer and a Second Output layer, which collectively culminate in the generation of the final predicted result. The hyperbolic sigmoid function is the activation function that is employed in the three layers. Nonlinearity has been included in these branches to enable the network to learn. The proposed model is flexible and can be adapted to include other performance metrics, such as radiation pattern, efficiency, or directivity, if required by specific design constraints.

2.4. Splitting a Data Set

The data set consists of three matrices with 256 samples for each, divided into three distinct cases: free space, with tissue, and with tissue inverse. Each case is further split into training, validation, and testing subsets according to a specified ratio. Specifically, 70% of the data is allocated to the training set, 15% to the validation set, and 15% to the testing set. This splitting ratio ensures that a significant portion of the data set is dedicated to training, which is crucial for the neural network to learn effectively. The effectiveness of the developed neural network model depends closely on this data allocation. The model's performance is defined by the relative root mean square error, where the relative mean square error (RMSE) is: Excellent $< 10\%$, Good $< 10\% < 20\%$, Fair $< 12\% < 30\%$, Poor $< 30\%$. The expression of mean square error is:

$$\text{RMSE} = \sqrt{\frac{1}{m}\sum_{j=1}^{m}(y_j - \hat{y}_j)^2} \tag{2}$$

where y is threshold values [37, 38].

3. APPLICATION EXAMPLES

To demonstrate the effectiveness of the three neural models described in the previous section, a rectangular patch microstrip antenna is used. The proposed antenna uses an FR-4 substrate with a thickness of 1.58 mm and a relative dielectric permittivity of 4.4. A trapped 50 Ω microstrip line is used to feed it. This type of antenna, characterized by its compact size, design flexibility, cost-effectiveness, and ability to integrate with other components, makes it an excellent choice for various applications, including biomedical ones. Simulations were carried out using HFSS software.

The antenna size parameters are summarized in Table 1. Six geometrical parameters were used to generate the data set. The obtained values of S_{11}, gain, and SAR are recorded to form the desired antenna performances. The inverse modeling using a neural network model consists of exchanging the inputs with the outputs so as to establish the relationship between the desired performances taken as inputs and the corresponding geometrical parameters taken as outputs. In this case study, the six geometrical parameters predicted by the proposed neural models are $t = [df, ex1, ex2, xpf1, xpf2, Lg]$, and these parameters are illustrated in Figure 5. The minimum and maximum values as well as the incremental step are given in Table 2.

TABLE 1. Antenna size parameter.

Paramater	dimension
W	13
L	12
Yf	12.5
Wsub	20
Lsub	24
H	1.58
T	0.035

TABLE 2. Training data of geometrical variables in (mm).

geometrical variables	min	max	step
df	-2	2	4
ex1	0.5	3.5	1
ex2	1.5	4.5	1
xpf1	13.5	16	2.5
xpf2	10	14	4
Lg	5	15	10

In this study, three cases are considered: in the first case, the antenna is placed in free space; in the second, it is placed on top of a model made up of three layers imitating the human body

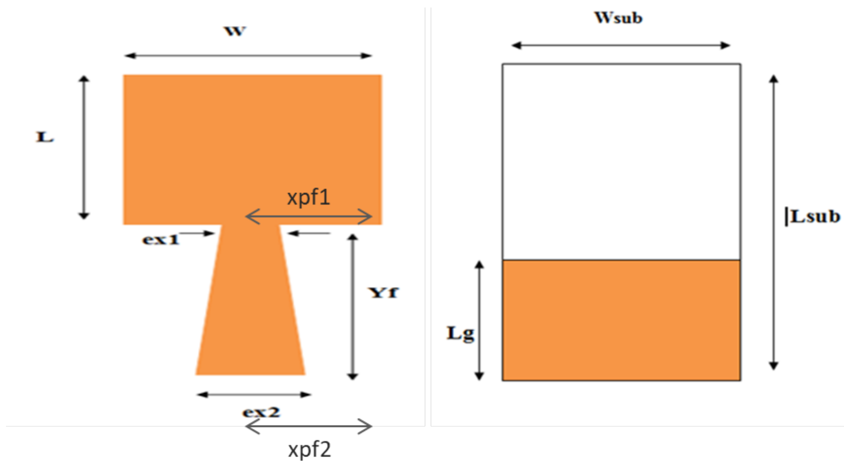

FIGURE 5. The proposed antenna's front and back views in HFSS.

FIGURE 6. Representation of a human tissues model.

in this case, the ground plane facing the ghost; in the third case, the antenna is inverted, and it is the patch that faces the human model.

Figure 6 illustrates the phantom model, which consists of three distinct layers representing the skin, fat, and muscle.

The dielectric properties of the human tissues used in this study are given in Table 3, and they were taken from [39]. However, for more accurate SAR evaluation, these properties can be experimentally measured using different techniques such as the open-ended coaxial probe method, as demonstrated in [40].

TABLE 3. Material properties of the human body.

	Skin	Fat	Muscle
Conductivity (s/m)	3.0608	0.24222	4.0448
Relative permittivity	35.7	5.0291	49.54
Loss tangent	0.3076	0.17315	0.29353

3.1. Specific Absorption Rate

Specific absorption rate is a metrics that uses radio frequency (RF) to determine the rate at which the body absorbs energy in response to an electromagnetic field.

$$\mathrm{SAR} = \frac{\sigma E^2}{\rho} \tag{3}$$

where E is the intensity of the electric field, ρ the tissue's mass density, and σ the conductivity. When measuring SAR, the apparatus is used at its intended capacity and transmits at maximum power. SAR is averaged over a tissue volume, usually 1 gram or 10 grams, because the electric field is normally not spatially homogeneous. Additionally, the E field is typically not constant over time, and time-averaging is done by the probe [41]. The following formula, which makes use of the definition of SAR, is used to determine the point SAR at the specified position r:

$$\mathrm{SAR}_{\mathrm{pnt}}(r,\theta) = \frac{\sigma E^2(r)}{\rho} \tag{4}$$

$$= \sigma\rho\left[|s_{11}|+|s_{22}|+2|s_{12}|\cos(\theta+\theta_0)\right] \tag{5}$$

The formula for point SAR_{pnt}, as given in (5), is applied at point r as a function of the phase difference θ between the excitation antennas. The following formula is used to calculate the volume-averaged SAR:

$$\mathrm{SAR}_{\mathrm{avg}}(\theta) = \frac{1}{v}\int \mathrm{SAR}_{\mathrm{pnt}}(r,\theta)\,\mathrm{d}r \tag{6}$$

4. RESULTS AND DISCUSSIONS

To show the close relationship between antenna performances with these geometric parameters, a parametric study was conducted over a wide frequency range by varying key design parameters, such as feed width, feed position, ground plane length, and feed line displacement from center. The results, illustrated in Figure 7, demonstrate how these parameters affect the impedance matching of the antenna, operating frequency band, and frequency bandwidth. The resulting data was then incorporated into the artificial neural network (ANN) training data set to enable accurate performance prediction and optimization. This approach ensures that the ANN effectively captures the relationship between geometric variations and antenna characteristics, thereby facilitating the efficient design of antennas for biomedical applications.

The study utilized three different ANN models: the first model, the second model, and the proposed model. Each model was tested under three conditions: in free space, with tissue, and with tissue inverse. The parameters of interest included the

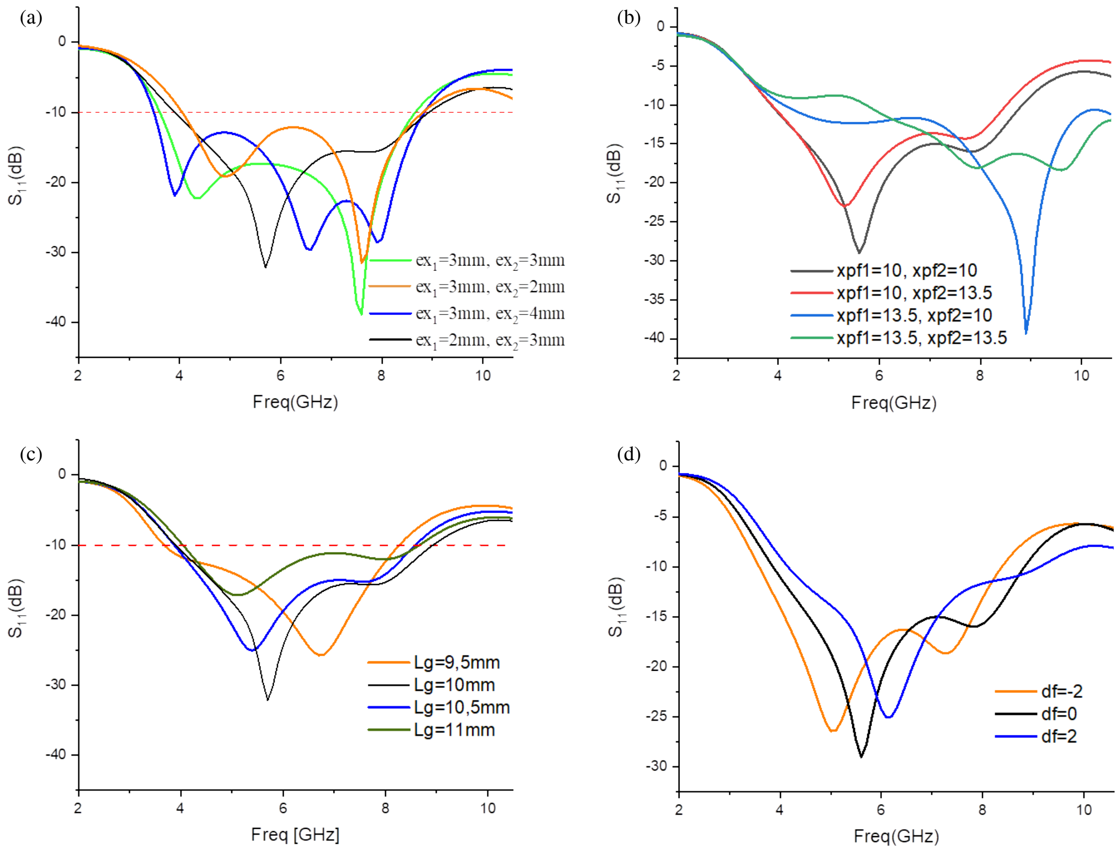

FIGURE 7. Parametric analysis of antenna performance: (a) Effect of feed width, (b) Effect of feed position, (c) Effect of ground plane length, (d) Effect of feed line displacement from the center.

reflection coefficient S_{11}, gain, and Specific Absorption Rate (SAR). The geometrical variables were obtained through training and were used to create antenna structures. The synthesis consists of inputting the reflection coefficient S_{11} to get the geometrical dimensions $[df,\ ex1,\ ex2,\ xpf1,\ xpf2,\ Lg]$. Our objective was to evaluate each suggested model's performance compared with the others, which are [0, 2, 3, 10, 10, 10]. These geometrical variables obtained are not included in the training set.

4.1. Results Obtained in Free Space

Figure 8 presents the reflection coefficient (S_{11}) results obtained from simulations using HFSS and predictions from three different models of ANN: the first model, the second model, and the proposed model, in a free-space environment. The graph clearly shows how the proposed ANN model (green line) aligns closely with the HFSS simulated results (black line) across the frequency range of 0.6 to 10.6 GHz, indicating improved accuracy and reliability over the first model (red line) and second models (blue line). The proposed model's ability to maintain low reflection coefficients at key frequencies demonstrates its effectiveness in optimizing antenna design, particularly around the resonant frequencies where minimal reflection is desired. Figure 9 illustrates the gain results achieved using HFSS simulations compared to the predictions made by three ANN models: the first model, the second model, and the proposed model, in free space. The proposed ANN model (green line) shows a gain pattern that closely follows the HFSS results (black line) in the entire frequency band, showcasing its enhanced predictive capability. The proposed model's improved gain predictions over the entire frequency spectrum, especially around the resonance points, highlight its efficiency in antenna design optimization. This enhanced gain consistency across different frequencies reflects the proposed model's superior performance compared to the first (red line) and second models (blue line).

4.2. Results Obtained with Tissue

The introduction of the phantom causes a frequency shift towards the low frequencies, as illustrated by Figure 10. As the frequency band in this study is fixed for all generated data (ranging from 0.6 GHz to 10.6 GHz with a step of 0.1 GHz), the frequency shifting manifests itself in the S_{11} parameter, which does not start from 0 dB but at a lower value that is not taken into account in the considered frequency band. The effectiveness of the proposed neuronal model is more apparent in the case with tissue. In fact as shown in the results of Figure 10, a narrow band behavior is achieved in the case of the first and second models with a peak around 1 GHz, while the results obtained with the proposed neural model follow the pattern of those obtained with HFSS with a wider bandwidth for the proposed model.

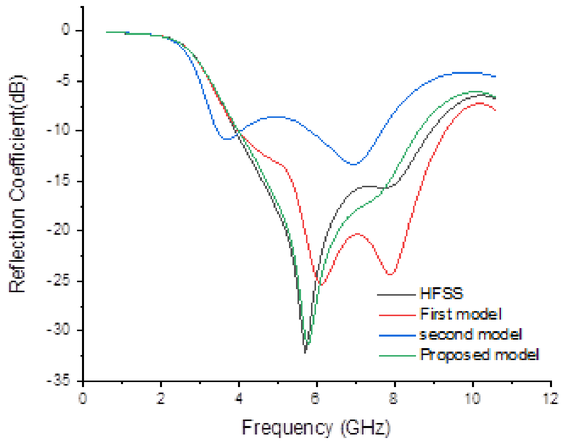

FIGURE 8. Results of reflection coefficient obtained using HFSS and ANN models in free space.

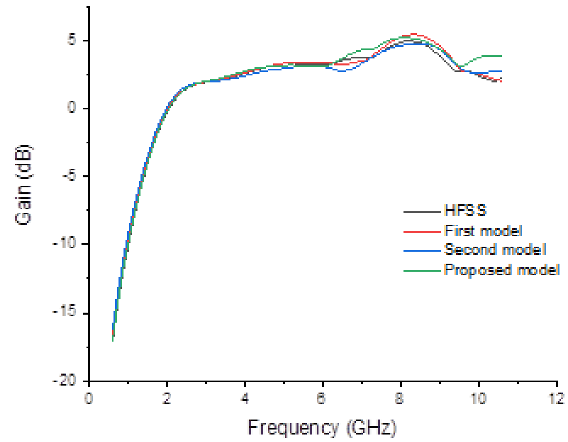

FIGURE 9. Results of gain obtained using HFSS and ANN models in free space.

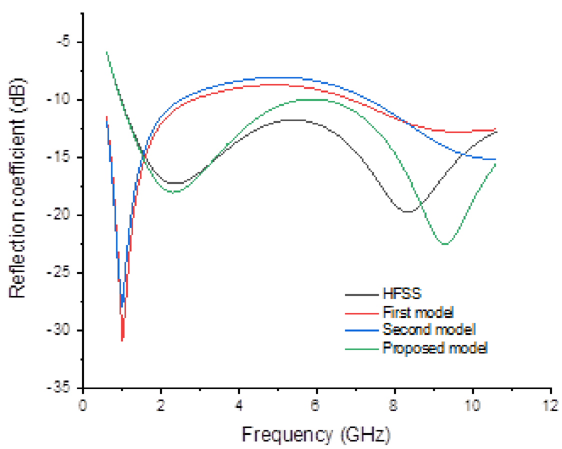

FIGURE 10. Results of reflection coefficient obtained using HFSS and ANN models with tissue.

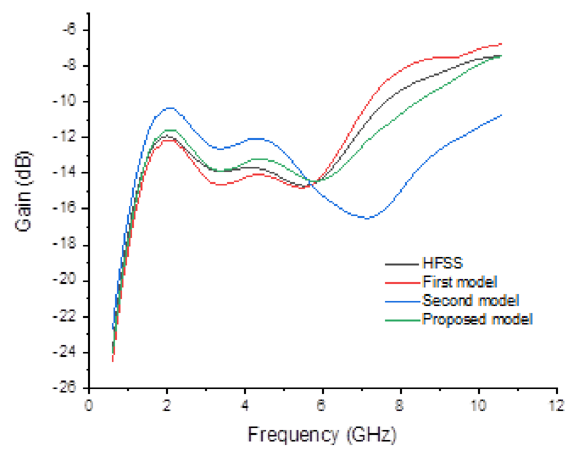

FIGURE 11. Results of gain obtained using HFSS and ANN models with tissue.

Figure 11, depicting gain versus frequency, demonstrates that the proposed ANN model aligns closely with the HFSS benchmark, achieving consistent and high gain values across the frequency range, same observation for the first model. In contrast, the second ANN model exhibits significant deviations, particularly at frequencies above 6 GHz.

Figure 12 shows SAR versus frequency, where lower values are crucial for safe biomedical applications. The proposed ANN model again excels, closely matching the HFSS SAR values and indicating safer energy absorption levels. The first ANN model shows significantly higher SAR values, and while the second ANN model is improved, it still exceeds the benchmark. Overall, the proposed ANN model consistently shows the best performance across all parameters, making it the most optimized and suitable choice for biomedical applications among the evaluated models. Overall, the proposed ANN model consistently shows the best performance across all parameters, making it the most optimized and suitable choice for biomedical applications among the evaluated models.

4.3. Results Obtained with Tissue Inverse

In Figure 13, which shows the reflection coefficient versus frequency, the proposed model closely matches the HFSS results, especially at lower frequencies (below 4 GHz). There are minor deviations between the models, particularly between 4 GHz and 8 GHz, but all models exhibit similar trends, indicating that the proposed model is a good approximation of the HFSS results.

In Figure 14, which presents gain versus frequency, the gain values of the proposed model are quite close to the HFSS results over the entire frequency range. The second model also presents results very comparable to those of the HFSS, and the greatest deviation is recorded by the first model, especially for high frequencies.

The results obtained for the SAR, Figure 15, confirm those obtained for the two previous performances, namely S_{11} and gain. Indeed, once again, the results obtained by the proposed model closely follow those of HFSS followed by those of the second model, while the first model records the largest deviation.

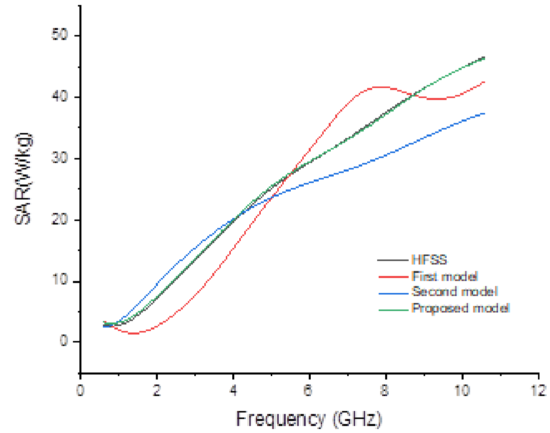

FIGURE 12. Results of SAR obtained using HFSS and ANN models with tissue.

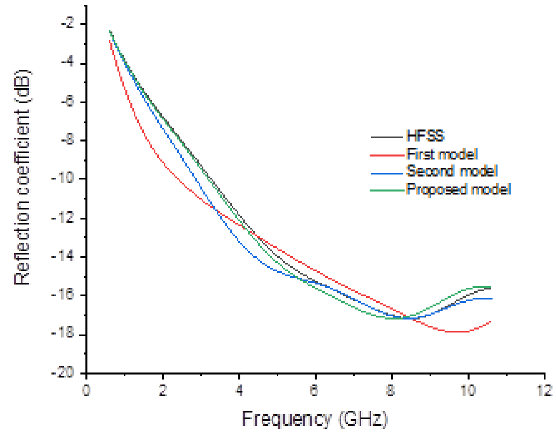

FIGURE 13. Results of reflection coefficient obtained using HFSS and ANN models with tissue inverse.

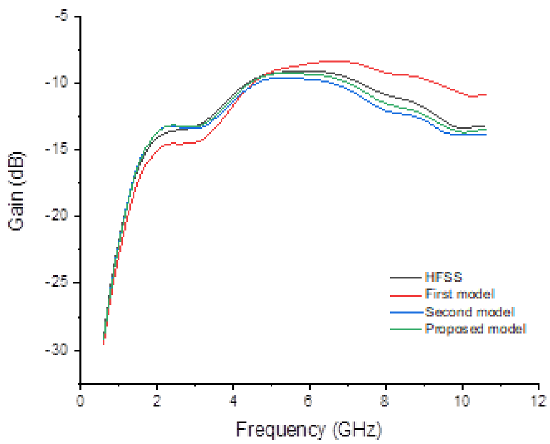

FIGURE 14. Results of gain obtained using HFSS and ANN models with tissue inverse.

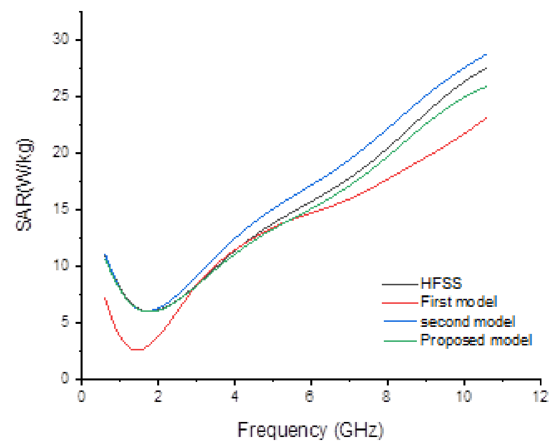

FIGURE 15. Results of SAR obtained using HFSS and ANN models with tissue inverse.

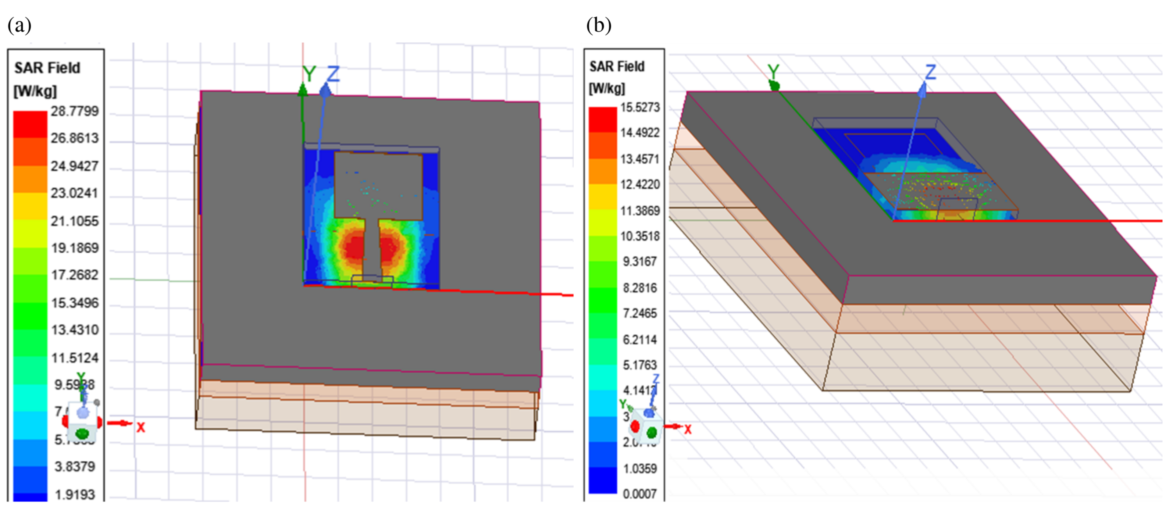

FIGURE 16. Results of SAR average in frequency 5.8 GHz obtained using HFSS (a) with tissue (b) with tissue inverse.

According to the results illustrated in Figure 16, the SAR value recorded at the 5.8 GHz frequency is 28.7799 W/kg with fabric, 15.5273 W/kg with reverse fabric, and it increases with

TABLE 4. Geometrical parameters predicted using the first model.

	Free space	With tissue	With tissue inverse
input is S_{11}	0.2859	−0.4013	0.3137
	1.9373	1.8994	0.7653
	2.9819	2.7466	1.9363
	9.118	10.0167	9.9384
	9.9572	10	9.8151
	9.8597	5.5996	8.7726
RMSE	0.3842	1.8074	0.8464
input is Gain	0.0309	0.0927	0.676
	1.8412	1.8320	1.8976
	2.429	2.0636	2.8036
	10.0559	11.1748	8.5928
	9.6690	10.9912	9.7212
	9.6635	11.6794	9.2837
RMSE	0.3104	1.0079	0.7161
input is SAR	-	1.3271	0.4741
		3.2753	2.158
		1.0725	2.3389
		8.3203	10.9831
		9.548	9.998
		15.1989	9.1571
RMSE	-	2.4885	0.6277

TABLE 5. Geometrical parameters predicted using the second model.

	Free space	With tissue	With tissue inverse
inputs are S_{11}, Gain, and SAR	0.003	−0.0035	0.2595
	2.024	1.8098	1.6326
	3.032	2.8193	2.8892
	9.9779	9.96	9.7353
	10.0166	9.9553	9.7598
	7.8817	5.3274	10.551
RMSE	0.8650	1.9107	0.3281

TABLE 6. Geometrical parameters predicted using the proposed model.

	Free space	With tissue	With tissue inverse
inputs are S_{11}, Gain, and SAR	0.0049	0.99	−0.3388
	1.9216	1.7506	1.9679
	2.8299	3.2502	3.0113
	10.0559	10.0112	10.0349
	9.9695	10.1063	10.0736
	9.8645	10.0218	9.8375
RMSE	0.0979	0.4314	0.1576

increasing frequency. In this present work, we studied the DAS over the entire frequency range. To limit the SAR, it has been reported in the literature [42–44] that it can be limited by limiting the power supplied to the antenna. To determine the power input required to achieve a specific absorption Rate value (SAR), we can use the formula:

$$\mathrm{SAR} = \frac{P}{m} \tag{7}$$

P represents the power absorbed by the tissue, measured in watts (W), and m denotes the mass of the tissue, measured in kilograms (kg). So, the estimated power input for a SAR of 28 W/kg at 5.8 GHz, given a hand mass of approximately 0.0412 kg, would be approximately 1153.6 mW. In tissue, it is approximately 639.72776 mW.

Figure 16 illustrates average SAR results in frequency 5.8 GHz obtained using HFSS with tissue and with tissue inverse.

From all the comparisons carried out in the three cases studied: free space, with tissue, and with tissue inverse, it is clear that the proposed neural model manages to closely predict the results of the HFSS simulation. This shows that this model can predict, with good precision, the geometric parameters of the antenna for all the desired performances. It also demonstrates that the proposed model is a reliable alternative to HFSS simulations because it provides accurate instantaneous approximations.

To show the performance of the designed antenna in terms of radiation, the E plane and the H plane radiation patterns were plotted for the frequencies 3.6 GHz, 5.8 GHz, and 8.3 GHz covering the entire frequency range and for the three cases studied, namely free space, on the tissue, and on the tissue inverse. These diagrams illustrated in Figure 17 are obtained by HFSS simulation and not by neural models. A quasi-omnidirectional radiation pattern is obtained in both planes. A slight increase in gain can be seen in the case with tissue and with tissue inverse because of the reflection at the air/skin interface. Stability of the diagrams over the entire frequency range was also observed.

The results reported in Tables 4, 5, and 6 highlight the performance of three neural models in predicting geometric variables under various conditions. The maximum value of the RMSE recorded by the first model is 2.4885 (SAR as inputs) in the case of tissue, and its minimum value is 0.3104 (gain as inputs) recorded in the case of free space (Table 4). The second neural model recorded a maximum RMSE of 1.9107 (S_{11}, gain, and SAR as inputs) in the case with tissue and a minimum value of 0.3281 in the case with inverse tissue (Table 5). The proposed model recorded a maximum RMSE of 0.4314 in the case with tissue and a minimum RMSE of 0.0979 obtained in the case of free space. These results confirm that the proposed model is very effective in predicting geometric variables with high accuracy, even when the antenna is placed on tissue, making it a reliable choice for antenna design and optimization.

A comparison in terms of size, bandwidth, gain, and SAR is carried out between this present work and some works taken from the literature, and this comparison is reported in Table 7. The designed antenna combines very good performances with an acceptable SAR compared to other works.

The prototype of the manufactured antenna placed on the rear arm is illustrated in Figure 18. The simulation results were

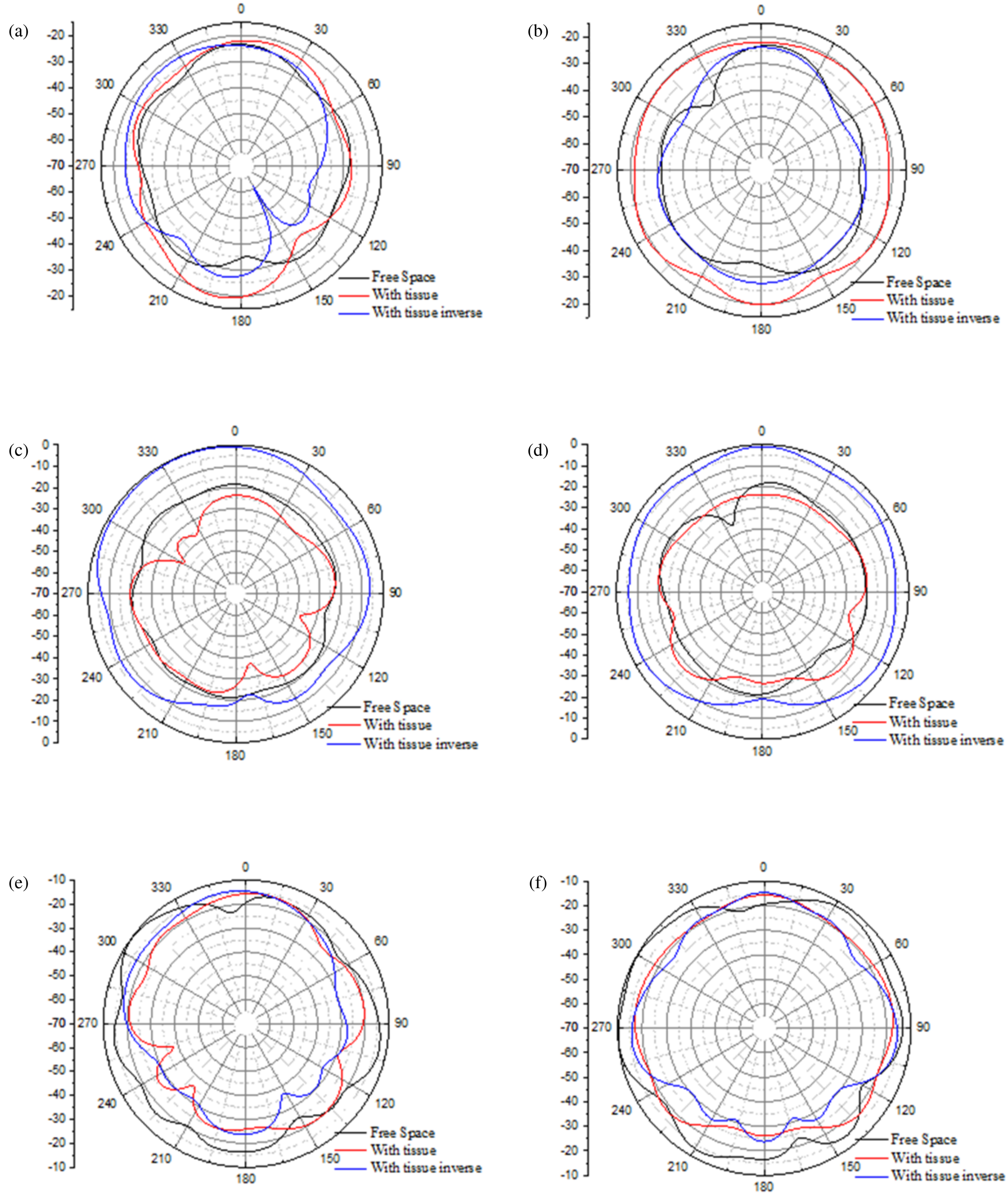

FIGURE 17. Radiation pattern of the first antenna structure according to the three possibilities for the frequencies 3.6 GHz. ((a) E-plane, (b) H-plane), 5.8 GHz ((c) plane E, (d) plane H) and 8.3 GHz ((e) plane E, (f) plane H).

compared to those of the measurement and are reported in Figure 19. A good agreement between the simulation results and measurements is observed. The recorded offset is due to several factors, namely: in the simulation the antenna is placed horizontally 2 mm above a planar phantom of rectangular shape of finite dimensions with three layers whose dielectric parameters are fixed (the frequency dependence is not taken into account) while the measurements are carried out directly on the forearm of an adult, with a shirt as the separation between the skin and the ground plane whose dielectric properties are unknown and are not taken into account during the simulation, in addition to other factors, namely wiring, connections, equipment, etc.

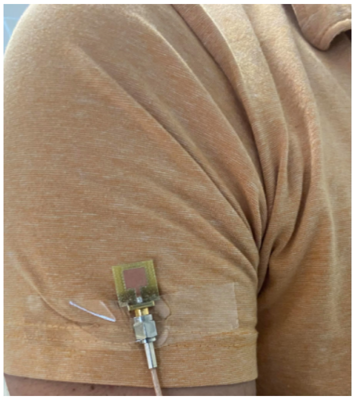

FIGURE 18. Photos of the prototypes fabricated antenna.

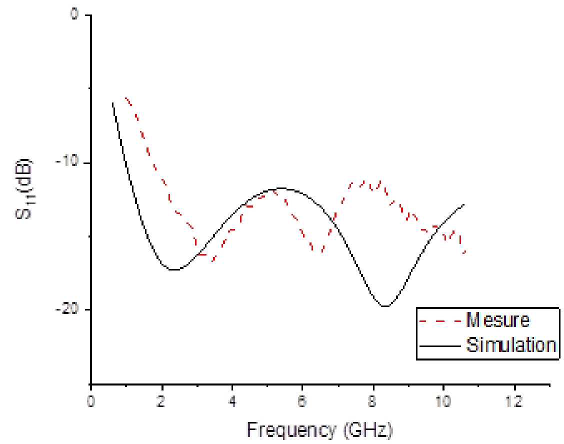

FIGURE 19. Reflection coefficient measured and simulation results.

TABLE 7. Comparison with other works.

Reference	Size (mm^3)	Size (λ_{eff})	BW (GHz)	Gain (dB)	SAR (W/kg)
[45]	$40.5 \times 40.5 \times 6$	$1.30 \times 1.30 \times 0.19$	5.5–6.06	7.47	46.9
[46]	$30 \times 34 \times 0.8$	$0.60 \times 0.68 \times 0.016$	4.3–5.9	1.56	14.1
[47]	$102 \times 68 \times 3.6$	$2.92 \times 1.95 \times 0.103$	5.07–5.35	6.12	47.26
[48]	$5 \times 7 \times 0.3$	$0.159 \times 0.222 \times 0.010$	4.82–6.97	-	826
[49]	$47 \times 37 \times 1.6$	$1.41 \times 1.11 \times 0.048$	5.70–5.91	7	-
[50]	$51 \times 51 \times 5$	$1.00 \times 1.00 \times 0.098$	5.77–5.9	8.87	-
Our work	$20 \times 24 \times 1.58$	$0.81 \times 0.97 \times 0.064$	**3.86–8.83**	**3.2**	**28.78**

5. CONCLUSION

To reduce the simulation effort and time during antenna design, a multi-objective inverse artificial neural network (MOIANN) is proposed in this research. To better demonstrate the effectiveness of the proposed model, two other neural models were also studied. In the first model, the desired performances were presented separately while in the second they are presented simultaneously in a single block to create networks capable of predicting the geometric parameters of the antenna. In the proposed model, each performance is connected by a local layer independent of that of the other performances; then, the outputs of the three local layers are connected via a fully connected layer to establish the relationships between different performances. The superiority of this proposed technique is proven via all the comparisons carried out. Future work will explore integrating additional constraints, such as radiation pattern and directivity, for broader applicability in various biomedical and wireless communication scenarios.

REFERENCES

[1] Alenoghena, C. O., H. O. Ohize, A. O. Adejo, A. J. Onumanyi, E. E. Ohihoin, A. I. Balarabe, S. A. Okoh, E. Kolo, and B. Alenoghena, "Telemedicine: A survey of telecommunication technologies, developments, and challenges," *Journal of Sensor and Actuator Networks*, Vol. 12, No. 2, 20, 2023.

[2] Stuchly, M. A., "Biomedical concerns in wireless communications," *Critical Reviews™ in Biomedical Engineering*, Vol. 26, No. 1-2, 117–151, 1998.

[3] Malik, N. A., P. Sant, T. Ajmal, and M. Ur-Rehman, "Implantable antennas for bio-medical applications," *IEEE Journal of Electromagnetics, RF and Microwaves in Medicine and Biology*, Vol. 5, No. 1, 84–96, 2020.

[4] Kim, H.-J., H. Hirayama, S. Kim, K. J. Han, R. Zhang, and J.-W. Choi, "Review of near-field wireless power and communication for biomedical applications," *IEEE Access*, Vol. 5, 21 264–21 285, 2017.

[5] Rahmat-Samii, Y. and J. Kim, *Implanted Antennas in Medical Wireless Communications*, Springer Nature, 2022.

[6] Sumithra, P. and D. Thiripurasundari, "Review on computational electromagnetics," *Advanced Electromagnetics*, Vol. 6, No. 1, 42–55, 2017.

[7] Liu, C. and R. G. Kelly, "A review of the application of finite element method (FEM) to localized corrosion modeling," *Corrosion*, Vol. 75, No. 11, 1285–1299, 2019.

[8] Teixeira, F. L., C. Sarris, Y. Zhang, D.-Y. Na, J.-P. Berenger, Y. Su, M. Okoniewski, W. C. Chew, V. Backman, and J. J. Simpson, "Finite-difference time-domain methods," *Nature Reviews Methods Primers*, Vol. 3, No. 1, 75, 2023.

[9] Zhang, S., C. Zhang, Q.-J. Zhang, *et al.*, "Parallel computational approach to gradient based EM optimization of passive microwave circuits," *IEEE Transactions on Microwave Theory and Techniques*, Vol. 64, No. 1, 44–59, 2015.

[10] Bakr, M. H., J. W. Bandler, M. A. Ismail, J. E. Rayas-Sanchez, and Q.-J. Zhang, "Neural space-mapping optimization for EM-based design," *IEEE Transactions on Microwave Theory and Techniques*, Vol. 48, No. 12, 2307–2315, 2000.

[11] El Misilmani, H. M., T. Naous, and S. K. A. Khatib, "A review on the design and optimization of antennas using machine learning algorithms and techniques," *International Journal of RF and Microwave Computer-Aided Engineering*, Vol. 30, No. 10, e22356, 2020.

[12] Abdolrasol, M. G. M., S. M. S. Hussain, T. S. Ustun, M. R. Sarker, M. A. Hannan, R. Mohamed, J. A. Ali, S. Mekhilef, and A. Milad, "Artificial neural networks based optimization techniques: A review," *Electronics*, Vol. 10, No. 21, 2689, 2021.

[13] Agatonovic-Kustrin, S. and R. Beresford, "Basic concepts of artificial neural network (ANN) modeling and its application in pharmaceutical research," *Journal of Pharmaceutical and Biomedical Analysis*, Vol. 22, No. 5, 717–727, 2000.

[14] Sran, S. S. and J. S. Sivia, "ANN and IFS based wearable hybrid fractal antenna with DGS for S, C and X band application," *AEU — International Journal of Electronics and Communications*, Vol. 127, 153425, 2020.

[15] Kumar, R., P. Kumar, S. Singh, and R. Vijay, "Fast and accurate synthesis of frequency reconfigurable slot antenna using back propagation network," *AEU — International Journal of Electronics and Communications*, Vol. 112, 152962, 2019.

[16] Malathi, P. and R. Kumar, "Design of multilayer rectangular microstrip antenna using artificial neural networks," *International Journal of Recent Trends in Engineering*, Vol. 2, No. 5, 53, 2009.

[17] Gopalakrishnan, R. and N. Gunasekaran, "Design of equilateral triangular microstrip antenna using artificial neural networks," in *IWAT 2005. IEEE International Workshop on Antenna Technology: Small Antennas and Novel Metamaterials*, 246–249, Singapore, Mar. 2005.

[18] Türker, N., F. Güneş, and T. Yildirim, "Artificial neural design of microstrip antennas," *Turkish Journal of Electrical Engineering and Computer Sciences*, Vol. 14, No. 3, 445–453, 2006.

[19] Thakare, V. V. and P. Singhal, "Microstrip antenna design using artificial neural networks," *International Journal of RF and Microwave Computer-Aided Engineering*, Vol. 20, No. 1, 76–86, 2010.

[20] Sağiroğlu, S., K. Güney, and M. Erler, "Resonant frequency calculation for circular microstrip antennas using artificial neural networks," *International Journal of RF and Microwave Computer-Aided Engineering*, Vol. 8, No. 3, 270–277, 1998.

[21] Baumgartner, P., T. Bauernfeind, O. Bíró, A. Hackl, C. Magele, W. Renhart, and R. Torchio, "Multi-objective optimization of Yagi–Uda antenna applying enhanced firefly algorithm with adaptive cost function," *IEEE Transactions on Magnetics*, Vol. 54, No. 3, 1–4, 2017.

[22] Chamaani, S., S. A. Mirtaheri, and M. S. Abrishamian, "Improvement of time and frequency domain performance of antipodal vivaldi antenna using multi-objective particle swarm optimization," *IEEE Transactions on Antennas and Propagation*, Vol. 59, No. 5, 1738–1742, 2011.

[23] Kabir, H., Y. Wang, M. Yu, and Q.-J. Zhang, "Neural network inverse modeling and applications to microwave filter design," *IEEE Transactions on Microwave Theory and Techniques*, Vol. 56, No. 4, 867–879, 2008.

[24] Xiao, L.-Y., W. Shao, F.-L. Jin, and B.-Z. Wang, "Multiparameter modeling with ANN for antenna design," *IEEE Transactions on Antennas and Propagation*, Vol. 66, No. 7, 3718–3723, 2018.

[25] Xiao, L.-Y., F.-L. Jin, B.-Z. Wang, Q. H. Liu, and W. Shao, "Efficient inverse extreme learning machine for parametric design of metasurfaces," *IEEE Antennas and Wireless Propagation Letters*, Vol. 19, No. 6, 992–996, 2020.

[26] Xiao, L.-Y., W. Shao, F.-L. Jin, B.-Z. Wang, and Q. H. Liu, "Inverse artificial neural network for multiobjective antenna design," *IEEE Transactions on Antennas and Propagation*, Vol. 69, No. 10, 6651–6659, 2021.

[27] Zhou, W.-Y., S.-Y. Sun, and M. Lu, "A novel metamaterial power divider optimized by artificial neural network," *AIP Advances*, Vol. 13, No. 4, 2023.

[28] Kaur, N., J. S. Sivia, and Rajni, "Artificial neural network based metasurface inspired planar frequency reconfigurable antenna for wireless applications," *International Journal of RF and Microwave Computer-Aided Engineering*, Vol. 31, No. 9, e22793, 2021.

[29] Kaur, M. and J. S. Sivia, "Giuseppe peano and cantor set fractals based miniaturized hybrid fractal antenna for biomedical applications using artificial neural network and firefly algorithm," *International Journal of RF and Microwave Computer-Aided Engineering*, Vol. 30, No. 1, e22000, 2020.

[30] Kaur, M. and J. S. Sivia, "ANN-based design of hybrid fractal antenna for biomedical applications," *International Journal of Electronics*, Vol. 106, No. 8, 1184–1199, 2019.

[31] Ali, D., T. Elwi, and S. Özbay, "Metamaterial-based printed circuit antenna for biomedical applications," *Avrupa Bilim ve Teknoloji Dergisi*, Vol. 26, 12–15, 2021.

[32] Rajawat, A. and S. H. Gupta, "Design and optimization of THz antenna for onbody WBAN applications," *Optik*, Vol. 223, 165563, 2020.

[33] Dhaliwal, B. S. and S. S. Pattnaik, "Development of PSO-ANN ensemble hybrid algorithm and its application in compact crown circular fractal patch antenna design," *Wireless Personal Communications*, Vol. 96, 135–152, 2017.

[34] Khan, T., A. De, and M. Uddin, "Prediction of slot-size and inserted air-gap for improving the performance of rectangular microstrip antennas using artificial neural networks," *IEEE Antennas and Wireless Propagation Letters*, Vol. 12, 1367–1371, 2013.

[35] Haykin, S., *Neural Networks: A Comprehensive Foundation*, Prentice Hall PTR, 1994.

[36] Chiroma, H., P. Nickolas, N. Faruk, E. Alozie, I.-F. Y. Olayinka, K. S. Adewole, A. Abdulkarim, A. A. Oloyede, O. A. Sowande, S. Garba, A. D. Usman, L. S. Taura, and Y. A. Adediran, "Large scale survey for radio propagation in developing machine learning model for path losses in communication systems," *Scientific African*, Vol. 19, e01550, 2023.

[37] Rabehi, A., A. Djebbari, A. Hafaifa, A. Souahlia, and A. Taleb-Ahmed, "New structure of CCR with an AOANN threshold," *Journal of Optical Communications*, Vol. 42, No. 1, 103–109, 2021.

[38] Prabhakar, D., P. Karunakar, S. V. R. Rao, and K. Srinivas, "Prediction of microstrip antenna dimension using optimized autometric Graph Neural Network," *Intelligent Systems with Applications*, Vol. 21, 200326, 2024.

[39] Karthik, V. and T. R. Rao, "Investigations on SAR and thermal effects of a body wearable microstrip antenna," *Wireless Personal Communications*, Vol. 96, 3385–3401, 2017.

[40] Khan, A., S. K. Dubey, and A. K. Singh, "Corner T-slot antenna at 2.45 GHz for hyperthermia application," *Journal of Electromagnetic Waves and Applications*, Vol. 38, No. 4, 508–521, 2024.

[41] Hochwald, B. M., D. J. Love, S. Yan, and J. Jin, "SAR codes," in *2013 Information Theory and Applications Workshop (ITA)*, 1–9, San Diego, CA, USA, Feb. 2013.

[42] Malik, N. A., P. Sant, T. Ajmal, and M. Ur-Rehman, "Implantable antennas for bio-medical applications," *IEEE Journal of Electromagnetics, RF and Microwaves in Medicine and Biology*, Vol. 5, No. 1, 84–96, 2020.

[43] Zada, M., I. A. Shah, and H. Yoo, "Metamaterial-loaded compact high-gain dual-band circularly polarized implantable antenna system for multiple biomedical applications," *IEEE Transactions on Antennas and Propagation*, Vol. 68, No. 2, 1140–1144, 2019.

[44] Rajagopalan, H. and Y. Rahmat-Samii, "Wireless medical telemetry characterization for ingestible capsule antenna designs," *IEEE Antennas and Wireless Propagation Letters*, Vol. 11, 1679–1682, 2012.

[45] Saha, P., D. Mitra, and S. K. Parui, "Control of gain and SAR for wearable antenna using AMC structure," *Radioengineering*, Vol. 30, No. 1, 81–88, 2021.

[46] Alemaryeen, A. and S. Noghanian, "On-body low-profile textile antenna with artificial magnetic conductor," *IEEE Transactions on Antennas and Propagation*, Vol. 67, No. 6, 3649–3656, 2019.

[47] Dam, T. H., M. T. Le, Q. C. Nguyen, and T. T. Nguyen, "Dual-band metamaterial-based EBG antenna for wearable wireless devices," *International Journal of RF and Microwave Computer-Aided Engineering*, Vol. 2023, No. 1, 2232674, 2023.

[48] Janapala, D. K. and M. Nesasudha, "A highly miniaturized antenna with wider band for biomedical applications," *Electromagnetic Biology and Medicine*, Vol. 41, No. 1, 35–43, 2022.

[49] Mondal, K., P. P. Sarkar, and D. C. Sarkar, "High gain triple band microstrip patch antenna for WLAN, Bluetooth and 5.8 GHz/ISM band applications," *Wireless Personal Communications*, Vol. 109, 2121–2131, 2019.

[50] Hake, S., R. Jaiswal, S. Moon, P. Nikam, and J. Kumar, "Performance enhancement of circularly polarized microstrip antenna using single-layer foam substrate for 5.8 GHz ISM band applications," *Telecommunications and Radio Engineering*, Vol. 84, No. 2, 43–65, 2025.